CANADA
DEPARTMENT OF ENERGY, MINES AND RESOURCES
Observatories Branch

PUBLICATIONS

of the

DOMINION OBSERVATORY

OTTAWA

Volume XXXIX • No. 11

THE BIAS IN dT/dΔ CALCULATED BY THE FAST CORRELATION METHOD FOR YELLOWKNIFE SEISMIC ARRAY DATA

D.H. Weichert

THE QUEEN'S PRINTER FOR CANADA
OTTAWA, 1970

Contents

THE BIAS IN dT/dΔ CALCULATED BY THE FAST CORRELATION METHOD FOR YELLOWKNIFE SEISMIC ARRAY DATA

D.H. Weichert

ABSTRACT: Automatic search-detection and processing of seismic events using a correlation technique has been used for several years for the data from the Yellowknife seismic array. Arrival vectors (azimuth and $dT/d\Delta$) of detected events are estimated from the parameters of the maximum correlation. The simple interpolation used to estimate the position of the maximum leads to a frequency-dependent bias. Estimates of the bias are presented for several frequencies. For teleseismic frequencies around 1 Hz, the computational bias in the fast processing algorithm of determining $dT/d\Delta$ varies from 0 to about 4 ms km^{-1}. An average scalar bias is 1.7 ms km^{-1}, which is smaller than the published error vectors in $dT/d\Delta$. These must therefore be explained by the structure of the earth.

RÉSUMÉ: Les données séismiques recueillies par le réseau séismique de Yellowknife sont automatiquement enregistrées et analysées depuis plusieurs années à l'aide d'une méthode de corrélation. Les vecteurs arrivées (azimut et $dT/d\Delta$) des phénomènes enregistrés sont calculés en fonction des paramètres de la corrélation maximale. L'interpolation simple utilisée pour déterminer la position du maximum entraîne une erreur systématique qui est fonction de la fréquence. L'auteur fait l'estimation de ces erreurs systématiques pour plusieurs fréquences. Dans le cas de fréquences téléséismiques de l'ordre de 1 Hz, l'erreur systématique du calcul de $dT/d\Delta$ par la méthode algorithmique rapide varie de 0 à environ 4 ms km^{-1}. L'erreur scalaire systématique moyenne est de 1.7 ms km^{-1}, et donc inférieure aux valeurs publiées du $dT/d\Delta$ des vecteurs erreurs. Ces erreurs ont donc leur origine dans la structure terrestre.

Introduction

The data from the Yellowknife seismic array were first processed at the Dominion Observatory in Ottawa in 1965. Initially strong emphasis was placed on the implementation of an automatic process to detect and locate low magnitude events, the process to be performed in real time or faster and still adequately cover the so-called Third Zone (the distance range from about 25° to 90° around the array) (Manchee and Somers, 1966). Based on the suggestions of Birtill and Whiteway (1965), correlations between the phased sums of two groups of seismometers were formed on a digital computer. The magnitudes of the correlations served as decision parameters for the presence of a seismic event in the original data. The phase lags corresponding to the maximum correlation were used as an estimate of the direction and velocity of the seismic energy arrival, and thus of the epicentre.

In 1966 a different algorithm for the calculation of cross correlations was implemented. With this algorithm, it became possible to increase the processing speed by a factor of two, without any significant sacrifice in the density of coverage of the Third Zone. Details of both methods have been described by Weichert, *et al.* (1967). To improve the crude estimate of the azimuth and $dT/d\Delta$ of the incoming seismic signal, a maximum in the two-dimensional correlation surface was calculated by interpolation from the three beams with the highest energy.

Weichert, *et al.* (1967) reported initial results obtained with the correlation program. They quoted rms errors in azimuth and range of epicentres, which were approximately equivalent to 3 to 5 ms km^{-1} errors in the measurement of $dT/d\Delta$. Manchee and Weichert (1968) reported similar errors, but also discovered pronounced regional trends in the errors. These authors recognized the bias inherent in their method of calculation, due to rounding in the calculation of lags in the first method, and to the asymmetry of the array response in both methods. They estimated the effect to be about 2 ms km^{-1} and concluded that it did not explain the epicentral errors. Indeed Weichert (1969) has shown, for events in Eastern Kazakh, that the regional trend of the error is caused by a systematic change of waveshape across the array, compared to which the computational bias is small. Mack (1969) described similar signal variations at the LASA in Montana. Further research into the causes of these effects will obviously require more refined methods of calculation than those used for the automatic search of the Yellowknife records. However, the fast correlation program has been extremely useful for its purpose and will most likely continue to be used at the Dominion Observatory, although modifications may be made from time to time. It is therefore important to understand the reasons for computational bias in the measurement of $dT/d\Delta$ by this method.

This paper presents a detailed numerical evaluation of the effects of the method of calculation, from which nominal corrections to the automatically calculated $dT/d\Delta$ can be obtained.

The Yellowknife Array Response

The response pattern of seismic arrays has been generally discussed by Birtill and Whiteway (1965). Somers and Manchee (1966) have given cross sections for constant azimuth and velocity of the Yellowknife array response for different processing methods. For our purposes it will be convenient to reformulate the well known results in vector notation.

A seismic wavefront arriving at the surface of the earth from a distant epicentre can be considered a plane, to a first approximation. We describe its linear intercept with the surface by the arrival vector s pointing into the direction of

arrival and having magnitude $dT/d\Delta$, which is the distance derivative of the seismic travel time. For convenience we assume initially a sinusoidal wave of frequency f. More realistic wavelets can then be considered via the superposition theorem. Assuming equal amplitudes on all channels, the signal arriving at the n^{th} seismometer at location $\mathbf{r}_n$ at time t is then represented by

$$y_n = \exp(i\omega(t + \mathbf{s} \cdot \mathbf{r}_n)) \tag{1}$$

If time delays corresponding to an arrival vector p are inserted in the channels of one array line and the seismometer outputs are then summed with unit weights, the resulting output is represented by

$$g = \exp(i\omega t) \sum_{n=0}^{N-1} \exp(i\omega(\mathbf{s}-\mathbf{p}) \cdot \mathbf{r}_0 n), \text{ where}$$

$\mathbf{r}_0$ is the constant unit separation between seismometers, N equals 10 for both lines of the YK array and the beginning of the line has been used as reference point. This expression is more conveniently written in the form

$$g = \exp\left(i\omega\left(t + \mathbf{q} \cdot \mathbf{r}_0 \frac{N-1}{2}\right)\right) \frac{\sin\left(\omega \mathbf{q} \cdot \mathbf{r}_0 \frac{N}{2}\right)}{\sin\ \omega \mathbf{q} \cdot \mathbf{r}_0/2} \tag{2}$$

where $\mathbf{q} = \mathbf{s} - \mathbf{p}$. The correlation between delayed sums along the NS (x = north) and the EW (y = east) lines are now formed by multiplying the individual sums, and averaging over a time T. (We ignore here a weighting factor used in the averaging process in the actual calculation in order to save computer memory.) Multiplying the real parts of the two line sums given by Equation (2), we obtain

$$G = D_x D_y \left(\cos 2\omega t' + \cos \omega \mathbf{q} \cdot \frac{(\mathbf{L}_x - \mathbf{L}_y)}{2}\right)$$

D_x and D_y are the diffraction patterns in the x and y directions appearing in Equation (2), $t' = t + \mathbf{q} \cdot \left(\frac{\mathbf{L}_x + \mathbf{L}_y}{2}\right)$ represents a time shift of the output which depends solely on the chosen space reference point, and $\mathbf{L}_x/2$ and $\mathbf{L}_y/2$ are the centre points of the two array lines. We shall replace $(\mathbf{L}_x - \mathbf{L}_y)/2$ by $\mathbf{R}$, the vector connecting the two line centres; numerically it is 1.25 km north and 6.25 km east. Averaging G over a time T, and omitting irrelevant time shifts gives

$$\bar{G} = D_x D_y \left(\cos \omega \mathbf{q} \cdot \mathbf{R} + \frac{1}{\omega T} \sin(\omega T) \cos(2\omega t')\right) \tag{3}$$

The moving average over the product of the phased line sums is seen to consist of a constant and a time variable term. The second term also depends on q and on the choice of reference point. For the usual averaging time of 1.6 s, its maximum value is about 10 per cent of the constant term, over the range of typical teleseismic frequencies (around 1 Hz), but with fixed T it depends strongly on frequency.

The coefficients D_x and D_y represent a two-dimensional diffraction pattern, which is symmetric because the line lengths are equal and contain the same number of seismometers. The first bracketed term compresses contours of this pattern slightly in the direction of R, which joins the centres of the array lines. The asymmetry in the second term will in general be different from that of the first, because of its complicated dependence both on q and on the reference point. To stabilize the correlation surface one would wish either to make the second term zero by proper choice of the averaging length, or to increase the averaging length until the second term becomes insignificant. The first method is impractical because $\sin \omega T/\omega T$ contains the unknown ω which varies with the seismic signal, and the second method introduces problems in the event detection process. A compromise for T between detection and automatic $dT/d\Delta$ estimation had to be found, and $T = 1.6$ s is generally used.

Only infinite sinusoids have been considered so far. Realistic seismic signals have finite energy and a definite onset time. As the signal moves across the array, the effective averaging time is initially zero, then increases to T. The second term in Equation (3) dominates therefore during the early part of the signal arrival, and this leads to strong oscillations in the correlation surface. This effect is demonstrated in a later section. For the purposes of the following discussions, the time variable part will mostly be ignored: its magnitude is often small, and the constant level of the correlation can be estimated if the correlation is available as a function of time.

The beam energy method of estimating the arrival vector consists in finding the coordinates of the maximum of the constant term of the correlation surface represented by Equation (3). Because of physical restrictions, array beams are formed only for a 20 X 20 ms km^{-1} grid, and the position of the maximum is estimated by a simple interpolation which is discussed later. Typical distances of the grid points from the centre of the diffraction response pattern are therefore about 0.01 km^{-1} at 1 Hz. At this distance a one-dimensional (single-line) diffraction pattern has decreased to about 90 per cent of its maximum value, while the strongest decrease of the asymmetric term, cos $\omega \mathbf{R} \cdot \mathbf{q}$, in the direction of R, is also about 90 per cent. Interpolations between beams with energy differences of this order can be expected to lead to reasonable estimates. As the frequency of the signal increases, however, the response pattern contracts relative to the beam grid, and justification of the simple interpolation becomes very difficult.

Use of the Fast Correlation Algorithm for $dT/d\Delta$ Estimation

This algorithm for beamforming and for the calculation of the correlation between the individual line sums of the two array arms was suggested by Weichert, *et al.* (1967). It was programmed in 1967 and has since been used for all routine processing of Yellowknife data. The program name is ARA.

The method is based on the highly regular geometry of the Yellowknife array (Weichert and Manchee, 1969), and on the results of early experiments which showed that the geology directly under the array must be highly uniform (Weichert and Whitham, 1969). For steeply arriving teleseismic wavefronts this means that time term corrections do not have to be applied to the signals from the individual seismometers.

Instead of forming beams for a given set of arrival conditions the signals from each line are summed for a given set of delays. The delays vary linearly along the line, and only integer values of the sampling interval are used. Finally, the delayed sums from the two lines are multiplied and averaged with a weighting function, resulting in a two-dimensional correlation matrix. The calculations are represented by

$$\text{sum}_{in}(t) = \sum_j \text{signal}_j(t - jn\,\Delta t) \qquad (4)$$

$i = 1, 2$ for the NS and EW array arms, $j = 1$ to 10 for the 10 seismometers in each line, and

$$C_{mn}(t) = C_{mn}(t-\Delta t) * (1-2^{-k}) + \text{sum}_{1m}(t) * \text{sum}_{2n}(t). \qquad (5)$$

The exponent $k(= 5)$ has been empirically selected: this makes the effective averaging length equal to 2^5 sampling intervals, or 1.6 *s* for routine teleseismic analysis ($\Delta t = 50$ ms).

The correlation matrix is interpreted as a measure of seismic energy arriving from the direction (m, n) in u-space (or $dT/d\Delta$ -space), that is with slowness components $m\Delta t/d$ and $n\Delta t/d$, where d is the 2.5-km seismometer spacing. The spacing of points in the correlation matrix therefore corresponds to 20 ms km^{-1} (2.22 *s* deg^{-1}) in travel time slope. Compared to the range of the travel-time slope over the Third Zone (approx. 80 to 40 ms km^{-1}), this spacing is much too large for a useful epicentre estimate. To obtain finer estimates of the coordinates of the correlation maximum, several approaches are possible. The correlation matrix can be defined and calculated on a finer grid. This would be achieved either by interpolating the data, or by rounding the required delays to the nearest available sampling points. Either method results in a substantial increase in calculation time and is therefore not practical for an automatic real-time, or faster, search of the entire Third Zone.

Another obvious approach is an interpolation of the correlation surface near the maximum. Ideally one would like to fit a scaled version of the theoretical correlation response to the points surrounding the maximum. This proves too cumbersome, because signal frequency and relative signal strength on different channels must be taken into account. Simpler quadratic least-squares fits have, therefore, been tried. Numerical experiments with several variations, paying attention both to calculation time and to performance, have led to the adoption of the simplest version: the coordinates of the maximum are estimated by two independent 3-point interpolations along the row and column of the maximum C_{mn} value, i.e.,

$$u_{x\max} = \Delta t/d \left(m + \frac{C_{m+1,n} - C_{m-1,n}}{2\,(2C_{m,n} - C_{m-1,n} - C_{m+1,n})} \right) \qquad (6)$$

with a similar expression for the y-component of the slowness. This method introduces a small bias into the result, because it presumes a symmetric parabola connecting the 3 points in either cross section, whereas the actual cross sections of the correlation surface are usually not symmetric. This bias has been shown to be proportional to the ratio of the third to second derivatives of the actual cross section (Wilson, 1965). A more severe effect of the asymmetry of the correlation response, given by Equation (3), is illustrated by Figure 1, which shows schematically the response of the YK configuration. The position of the actual maximum of any cross section deviates from the axis increasingly with the distance of the cross section from the origin of the response pattern. Of course, corrections or iterations could be used, but this would completely offset the advantage of simplicity of the interpolation estimate.

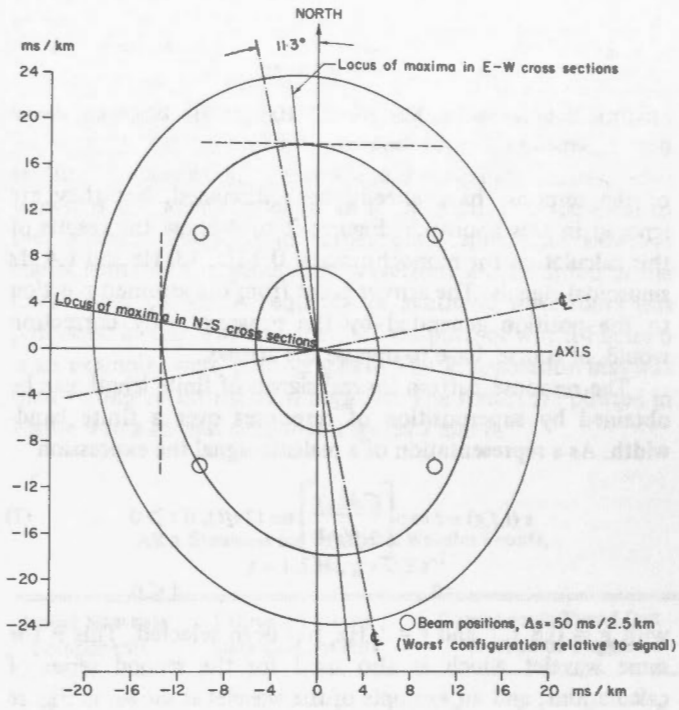

FIGURE 1. Schematic of the main lobe of the steady state correlation response of the Yellowknife seismic array at 1 Hz: the 95, 70 and 5- per cent power contours and the loci of maxima of NS and EW cross sections are indicated. The pattern is placed between four ARA beams (open circles), the worst location for both detection and interpolation.

Calculation of the Interpolation Bias

The actual magnitude and direction of the computational bias in the interpolation of arrival vectors by the standard ARA-program used at the Dominion Observatory is most easily estimated through numerical experiments. Two series of calculations have been made: one uses the constant term of the theoretical array response (Equation (3)) to predict the bias, while the other uses simulated noiseless wavefronts as input, both to the actual ARA program, and to a simulation of the ARA program. In all cases identical signal strengths and gains have been assumed for all channels.

In the first calculation the array response pattern is shifted relative to a 20 ms km^{-1} grid and its magnitudes at the neighbouring beams are calculated. Using Equation (6), an interpolated maximum position is obtained and compared with the originally assumed position. The difference is the interpolation bias. The problems due to the time-variable term

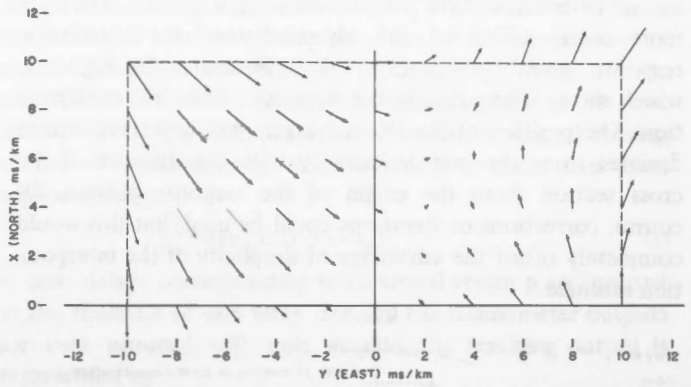

FIGURE 2. Interpolation bias for 0.7 Hz sinusoid based on steady state response.

of the response have already been discussed, but they are ignored in this approach. Figures 2 to 4 show the results of this calculation for monochromatic 0.7 Hz, 1.0 Hz and 1.4 Hz sinusoidal signals. The arrows point from the assumed position to the position generated by the program. Any correction would, of course, have to oppose the arrows.

The response pattern for real signals of finite length can be obtained by superposition of responses over a finite bandwidth. As a representation of a realistic signal the expression

$$s(t,f,g) = t \exp\left[\frac{-t^2}{2(f/g)^2}\right] \sin(2\pi f t), \text{ if } t > 0 \qquad (7)$$

$$= 0 \qquad t < 0$$

with $g = 0.8\ s^{-1}$ and $f = 1$ Hz, has been selected. This is the same wavelet which is also used for the second series of calculations, and an example of the wavelet is shown in Figure 6. The amplitude spectrum of the wavelet was obtained numerically, using a 50 ms sampling interval (64 points). Table 1 lists the component frequencies and their relative amplitudes down to the 1 per cent level. The response pattern was then calculated as a weighted sum over the component responses. Figure 5 shows the resulting steady state interpolation bias.

As explained above, the origins of the arrows in Figures 2 to 5 indicate the positions of the centres of the theoretical response pattern. The arrows point to the interpolated maxima. Only the upper half of a 20 by 20 ms km^{-1} square surrounding the beam at the origin is plotted. The values for the lower half of the square can be obtained by rotating the upper half by 180 degrees, because of the corresponding symmetry of the cosine term in the response. The bias for any arrival vector outside the plotted area is obtained by shifting the diagram to the beam with the maximum correlation, which is generally the beam nearest to the arrival vector. However, special care must be exercised in the regions that are centrally located between beams. Although the ideal pattern may result in a maximum value on one of the adjacent beams, noise may actually shift this maximum to another beam, resulting in an interpolation between a different set of beams than in the ideal case. The shift in the calculated maximum will then generally be greater than the small actual change in the correlation surface which caused it. Examples of this are discussed later.

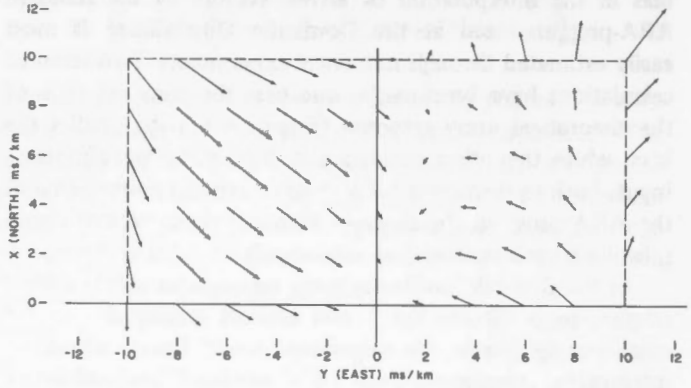

FIGURE 3. Interpolation bias for 1.0 Hz sinusoid based on steady state response.

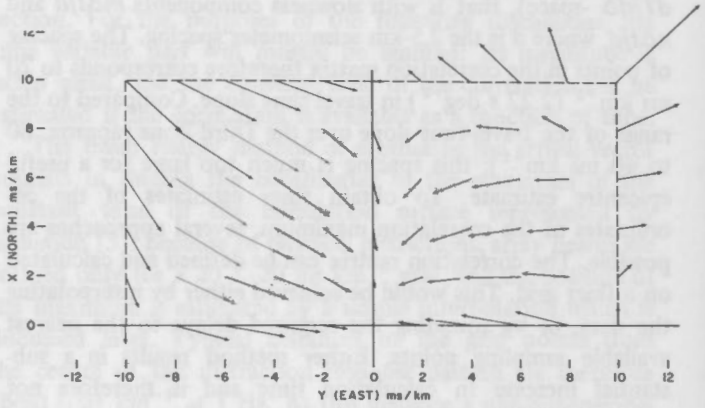

FIGURE 4. Interpolation bias for 1.4 Hz sinusoid based on steady state response.

The above discussion illustrates the origin of the interpolation bias and predicts its magnitude and direction. Although allowance is made for a real signal by using a broad band pattern in one case, the time-dependent part of the correlation function and the weighting factor for averaging are ignored. In order to check the theoretical predictions and the effect of this simplification, a series of synthetic noiseless events was generated on digital tape in the usual ARA format. These tapes were then processed by the standard ARA program. The seismic wavelet was represented by the Equation (7). An example of this wavelet is shown in Figure 6. The results of the experiment are listed in Tables 2 and 3, and are plotted in Figures 7 and 8. As in the earlier figures, the arrows point from the actual arrival vector to its interpolated position. The

Table 1

Normalized Amplitude Spectrum of Wavelet, $t \exp\left(\frac{-t^2}{2(f/g)^2}\right) \sin(2\pi t)$, $g = 0.8\ s^{-1}$, $f = 1$ Hz

Frequency	0.31	0.62	0.94	1.25	1.56	1.87	2.19	2.50	2.81
Amplitude	0.1	0.47	1.0	0.73	0.21	0.06	0.03	0.02	0.01

Table 2

ARA Slowness for Synthetic Wavelet Fronts, $f = 1.0$ Hz, $g = 0.8\ s^{-1}$

Actual Slowness Components		Estimated Steady State Components				Components Typed out at Time of Trigger			
s_x	s_y	s_x	s_y	Δs_x	Δs_y	s_x	s_y	Δs_x	Δs_y
				(ms km^{-1})					
−10.	−10.	− 7.8	−12.4	2.2	−2.4	− 7.8	−12.1	2.2	−2.2
−10.	− 5.	−10.5	− 3.0	−0.5	2.0	−10.8	− 3.9	−0.8	1.1
−10.	0.	− 9.5	− 0.6	0.5	−0.6	− 9.7	− 0.6	0.3	−0.6
−10.	5.	− 8.6	3.0	1.4	−2.0	− 8.9	2.9	1.1	−2.1
−10.	10.	− 7.8	8.0	2.2	−2.0	− 7.8	7.8	2.2	−2.2
− 5.	−10.	− 3.1	−10.5	1.9	−0.5	− 3.1	−11.4	1.9	−1.4
− 5.	− 5.	− 4.8	− 4.3	0.2	0.7	− 4.6	− 5.1	0.4	−0.1
− 5.	0.	− 4.2	− 0.2	0.8	−0.2	− 3.9	− 1.4	1.1	−1.4
− 5.	5.	− 4.0	3.0	1.0	−2.0	− 3.8	3.1	1.2	−1.9
− 5.	10.	− 3.2	8.2	1.8	−1.8	− 3.1	8.6	1.9	−1.4
0.	−10.	1.0	−11.0	1.0	−1.0	1.1	−10.8	1.1	−0.8
0.	− 5.	− 0.6	− 3.5	−0.6	1.5	− 0.3	− 4.2	−0.3	0.8
0.	0.	0.0	0.0	0.0	0.0	0.2	− 0.7	0.2	−0.7
0.	5.	0.6	3.8	0.6	−1.2	0.5	3.5	0.5	−1.5
0.	10.	1.0	9.4	1.0	−0.6	1.1	9.2	1.1	−0.8
5.	−10.	3.4	− 9.8	−1.6	0.2	3.2	− 9.8	−1.8	0.2
5.	− 5.	3.8	− 3.2	−1.2	1.8	4.0	− 4.4	−1.0	0.6
5.	0.	4.5	0.5	−0.5	0.5	4.4	− 0.3	−0.6	−0.3
5.	5.	5.0	4.0	0.0	−1.0	5.0	3.6	0.0	−1.4
5.	10.	3.4	10.4	−1.6	0.4	3.3	10.1	−1.7	0.1
10.	−10.	12.0	−12.0	2.0	−2.0	12.2	−12.2	2.2	−2.2
10.	− 5.	9.2	− 3.0	−0.8	2.0	9.2	− 3.9	−0.8	1.1
10.	0.	10.0	− 0.7	0.0	−0.7	10.3	− 0.6	0.3	−0.6
10.	5.	11.0	3.0	1.0	−2.0	11.0	2.9	1.0	−2.1
10.	10.	12.0	7.7	2.0	−2.3	12.2	7.8	2.2	−2.2

tables show, for the two different frequencies, the delays (slowness components) used for the generation of the digital data tape, and the interpolated coordinates for the correlation maximum. Two values are given: the second is the trigger value which is typed out by the ARA program at the time of event detection, while the first is the best estimate of the steady state value picked by eye from the processed traces. The two values differ slightly in most cases. This is partly due to the accuracy to which the slowness components can be estimated from the processed traces. The main reason is the oscillatory

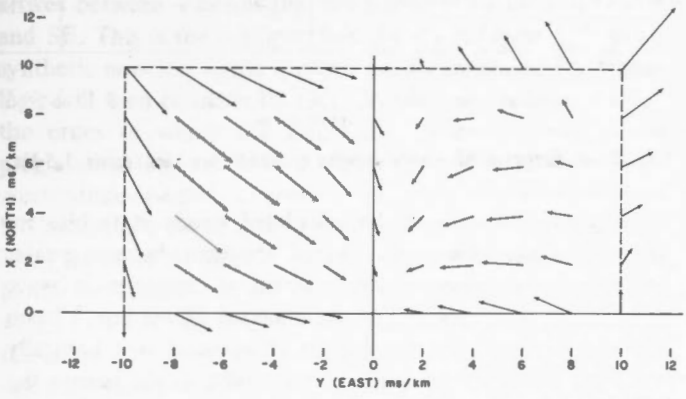

FIGURE 5. Interpolation bias for broadband signal, $f_0 = 0.94$ Hz, based on steady state response.

character of the actual correlation surface caused by the time-dependent term in Equation (3). The trigger logic of the ARA program makes no allowance for this oscillation, but simply assumes that the trigger delay of 1.6 s is sufficient for the oscillatory term to become negligible.

Figure 6 illustrates the effect of the oscillation in the correlation in two dimensions. A special program was written which simulates the ARA-processing of the ideal wavefront. Every 50 ms, as the wave passes the array, the maximum of the correlation surface is calculated by interpolation and plotted on a cathode ray tube. The actual delay components of the ideal wavefront are marked by an open circle. The coordinates of the correlation maximum after passage of the front are marked by a cross. To show the time sequence of the 2-D output, the NS and EW slowness components are plotted as time sequences in the top and right-hand margins. Also shown is the wavelet used as an ideal signal. It is identical to the wavelet described in earlier paragraphs. The slowness components of the generating wavefront are recorded in the lower right corner. A sequence of synthetic wavefronts was processed in this way and the CRT outputs, of which Figure 6 is an example, were photographed. The interpolation bias was then estimated on the film negative. The results are plotted in Figure 9 in a format similar to Figures 7 and 8.

Table 3

ARA Slowness for Synthetic Wavelet Fronts, $f = 1.5$ Hz, $g = 0.8\ s^{-1}$

Actual Slowness Components		Estimated Steady State Components				Components Typed Out at Time of Trigger			
s_x	s_y	s_x	s_y	Δs_x	Δs_y	s_x	s_y	Δs_x	Δs_y
				(ms km^{-1})					
−10.	−10.	− 7.5	−13.5	2.5	−3.5	− 7.5	−13.1	2.5	−3.1
−10.	− 5.	−11.0	− 1.8	−1.0	3.2	−11.1	− 1.9	−1.1	3.1
−10.	0.	− 9.8	− 0.2	0.2	−0.2	− 9.8	0.0	0.2	0.0
−10.	5.	− 8.7	1.7	1.3	−3.3	− 8.6	1.7	1.4	−3.3
−10.	10.	− 7.7	6.8	2.3	−3.2	− 7.6	6.9	2.4	−3.1
− 5.	−10.	− 2.8	−12.0	2.2	−2.0	− 2.8	−11.8	2.2	−1.8
− 5.	− 5.	− 4.0	− 2.5	1.0	2.5	− 4.0	− 2.5	1.0	2.5
− 5.	0.	− 3.6	0.0	1.4	0.0	− 3.4	− 0.2	1.6	−0.2
− 5.	5.	− 3.2	2.0	1.8	−3.0	− 3.1	1.7	1.9	−3.3
− 5.	10.	− 2.7	8.2	2.3	−1.8	− 2.8	8.1	2.2	−1.9
0.	−10.	0.6	−10.5	0.6	−0.5	0.5	−10.5	0.5	−0.5
0.	− 5.	0.0	− 1.8	0.0	3.2	− 0.1	− 2.2	−0.1	2.8
0.	0.	0.0	0.2	0.0	0.2	0.0	0.0	0.0	0.0
0.	5.	0.0	2.4	0.0	−2.6	0.2	1.9	0.2	−3.1
0.	10.	0.5	10.0	0.5	0.0	0.4	9.6	0.4	0.4
5.	−10.	2.5	− 9.0	−2.5	1.0	2.7	− 8.7	−2.3	1.3
5.	− 5.	3.0	− 1.8	−2.0	3.2	3.2	− 2.0	−1.8	3.0
5.	0.	3.0	0.0	−2.0	0.0	3.6	0.0	−1.4	0.0
5.	5.	4.0	2.5	−1.0	−2.5	3.9	2.2	−1.1	−2.8
5.	10.	2.2	11.0	−2.8	1.0	2.7	11.3	−2.3	1.3
10.	−10.	12.3	−13.3	2.3	−3.3	12.5	−13.2	2.5	−3.2
10.	− 5.	8.5	− 1.7	−1.5	3.3	8.9	− 1.9	−1.1	3.1
10.	0.	10.0	0.0	0.0	0.0	10.2	0.0	0.2	0.0
10.	5.	11.3	1.8	1.3	−3.2	11.4	1.7	1.4	−3.3
10.	10.	12.3	7.0	2.3	−3.0	12.5	6.9	2.5	−3.1

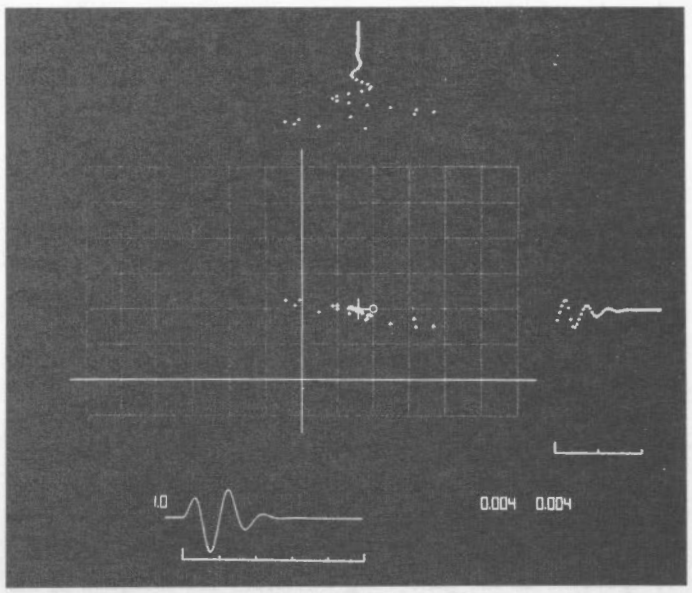

FIGURE 6. Sample output from ARA-simulation program. Grid spacing is 2 ms/km. True arrival of synthetic wavefront marked by open circle. Cross marks final location of maximum in correlation surface. The wavelet used for synthesis is shown in lower margin, with 5 *s* long time scale. The two-dimensional output is resolved into 1-component time sequences in the upper and right margins. Their time scale is shown in lower right margin. Below it are the coordinates of the synthetic wavefront in *s*/km.

Discussion

A cursory inspection of Figures 3, 7 and 9 reveals the basic similarity of the bias patterns as estimated by the different approaches. This establishes the validity of the steady state method. Figures 7 and 9 are really based on variants of the same method; they should therefore show the same pattern, as they very nearly do. In fact, the only reason for using the two variations was to check the simulation program with two-dimensional output against the ARA program. The obvious differences between the steady state and the synthetic wavefront approach lie along the outer boundaries and corners of the plotted 20 by 10 ms km^{-1} area which must be considered in order to include all possibilities occurring in a 20 by 20 ms km^{-1} beam grid spacing.

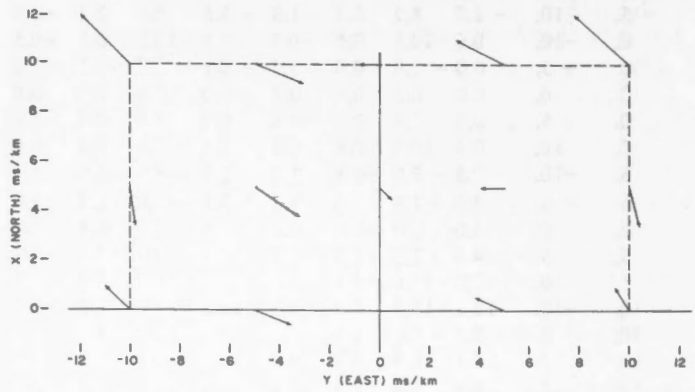

FIGURE 7. Errors in ARA slowness for synthetic wavelet fronts, 1 Hz.

Consider first the simpler steady state bias shown in Figure 3. Its amplitude and direction along the axes can easily be estimated from the YK-array response schematic in Figure 1. The response contours in this figure are shown as ellipses, but are only approximately so, near the response centre. For the present purposes the approximation is quite good at 1 Hz. For any event west of the beam with maximum energy, the NS interpolation will cut the actual pattern, due to the arriving signal on its east side. The true maxima of all such cross sections are south of the response centre, as shown by the respective locus in Figure 1. This corresponds to the negative bias in the x coordinate, west of the centre beam, as shown by Figure 3. The bias for events towards the north is similarly obtained from the locus of maxima in EW across sections. Since the beam is south of the response pattern, the bias is expected to be easterly and smaller than the x-bias at comparative distances from the beam. This is again confirmed by Figure 3. The good agreement of prediction from the schematic and the actual 3-point interpolation show that this interpolation is really quite effective, as long as the centre point is near one axis. As events move into the quadrants, and farther into the corners, distortions begin to appear, which cannot be predicted from the simple interpretation of Figure 1. They are caused by the symmetric interpolation over intervals of 20 ms km^{-1} in cross sections which are no longer symmetric.

In the NE quadrant of Figure 3 several arrows point outside the area belonging to the centre beam. This is the formal result of the simulated interpolation; however, in such a case, an ideal signal front should have maximum power on one of the adjacent beams, and the bias would have to be calculated with respect to that beam, resulting in a bias almost at right angles to the one shown in this figure.

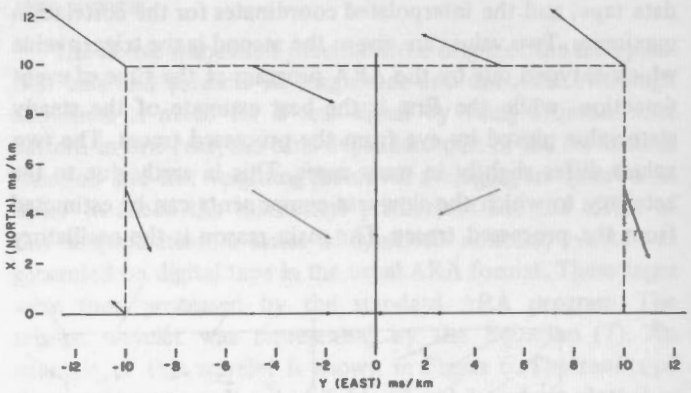

FIGURE 8. Errors in ARA slowness for synthetic wavelet fronts, 1.5 Hz.

Figures 2 to 4 show the calculated steady state bias for increasing frequencies. As predicted, the errors become greater because the response pattern which is constant in wave number, contracts relative to the constant 20 ms km^{-1} beam spacing. However, for the higher frequencies one naturally wishes to increase the sampling rate, which would narrow the beam pattern automatically. It is interesting in this connection to note that the results shown in Figure 3 for 1 Hz reflect the

decision to take 20 samples per second, i.e., per period, which is 10 times more than demanded by the Nyquist criterion of two samples per period of the highest frequency present in the signal. If the broadband nature of seismic signals is considered, our rate is still about 2 to 3 times the Nyquist sampling rate. To maintain the interpolation bias at the level of Figure 3 for higher dominant frequencies, the sampling rate must be increased proportionally. In Figure 5, the broadband bias centred on 0.94 Hz looks like a single frequency pattern, slightly above 1 Hz. This is doubtless due to the weighted summation of single frequency responses in which the higher frequencies dominate slightly. Figure 6 is a very good illustration of the effect of the time dependent term in Equation (3), which in this case is actually a transient. As predicted, the position of the maximum oscillates strongly as the signal passes over the array; as the effective averaging time lengthens, the amplitudes of the oscillation decrease and the position of the maximum becomes quite steady, at the value predicted by the constant term in Equation (3).

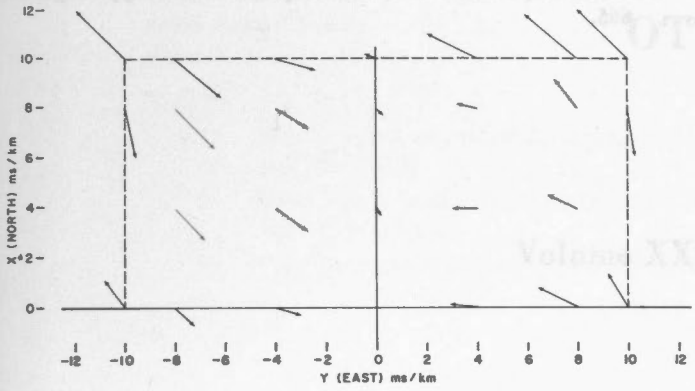

FIGURE 9. Interpolation bias from 2-D output of ARA simulation program for synthetic wavelet fronts, 1 Hz.

Returning to the comparison of Figures 3 and 9 the gross discrepancies half way between different beams must now be explained. In the NW corner Figure 3 shows a bias of about 2 ms km^{-1} pointing towards the centre beam, while Figure 9 shows an almost exactly opposite bias. For an event which arrives between 4 beams the two strongest beams will be NW and SE. This is the configuration shown in Figure 1. For the synthetic noiseless signal the two beams are equal. The trigger logic will then consistently pick the same beam, depending on the order in which the C-matrix is searched, and on the programmed inequality used for selecting the maximum (i.e., greater-than-or-equal, or greater than). The program selects the NW beam; relative to this beam the event is in the SE corner. The bias for this corner is obtained by a 180° rotation of the plotted values. It points toward the selected centre beam, which is NW of the plotted area and thus exactly opposite to the arrow shown in Figure 3. The same reasoning also explains not only the direction of the bias for the NE corner in Figure 9, but all other arrows along the boundaries which appear to disagree with the steady state bias, in Figure 3.

The region of the sharp switch from one direction of bias to another one should be somewhat smeared out by the noise background of real signals; however, it is quite real and could have been predicted from the steady state approach by comparing two diagonally adjoining diagrams, which predict opposite bias for the same point.

Manchee and Weichert (1968) published error vectors derived from the older correlation method which used a polar beam grid at equal azimuth and slowness. For instance, for two neighbouring source regions in the Aleutians they showed error vectors which on the average were at right angles to one another. Comparison with the beam pattern then used shows that one region was close to the north boundary of one beam area, and the second region was SE of the next beam; the errors were almost 10 ms km^{-1}. A nominal correction decreases the angle between the average error vectors in the two regions, but the difference is still significant. Moreover, the arrival vector anomaly for these regions, as well as for others, have been confirmed by least-squares calculations involving only the earliest parts of the signals. It is therefore clear that substantial anomalies remain which must be explained in terms of structure within the earth. The bias effect, although smaller than the anomalies, is of similar order of magnitude and must be considered in future large-scale experiments.

Conclusions

The method of interpolation used in the standard fast-correlation ARA-program, to obtain an improved estimate of the position of maximum correlation, introduces a bias into the results. For 1 Hz frequency this computational bias is generally about 2 ms km^{-1} but does reach 4 ms km^{-1} for the worst signal-beam configuration. The bias is largest in the NW and SE quadrants around any one beam, and pointing toward the beam. In the SW and NE quadrants the bias is small and swings slowly away from the beam. In the boundary region between beams the bias is indefinite since it depends on the selection of beams by the program logic. In these regions, small effects can reverse the bias. For higher frequencies the bias is stronger, unless the sampling rate is also increased, which decreases the grid spacing. Tables and diagrams of the bias for several frequencies and event-to-beam configurations have been given for constant signal strength across the array. Corrections to arrival vectors measured by this method should always be applied.

The bias originates from two causes: one is the shape and orientation of the centre lobe of the Yellowknife array response. It causes maxima of non-axial cross sections to shift away from the axes of the response. The second cause is the inefficiency of the interpolation used to locate the correct maximum of asymmetric cross sections far from the lobe centre and over the grid intervals used.

Both faults can be corrected by a denser grid spacing. This is not possible for a multiple-real-time speed process such as the ARA program. A slow version of this program has, therefore, been developed. Since it is many times slower than

real-time speed, data input must be from digital tape. Beams are formed for a fine grid of delays, surrounding the approximately known arrival vector, with a typically 1 or 0.5 ms km^{-1} spacing for each slowness component, or an equivalent spacing in azimuth and $dT/d\Delta$. This is believed to be near the useful limit for our array. For delays which are not integer multiples of sampling intervals, data points are interpolated linearly between the sampled values. Interpolations in the correlation surface are no longer necessary. For optimum epicentre location and for research measurements of $dT/d\Delta$ by the correlation method, this program should always be used after an event has been detected and digitized by the standard ARA program.

Acknowledgments

I am grateful to F.M. Anglin of the Seismology Division who wrote the plotting routines for our on-line cathode ray display, and to Dr. K. Whitham for carefully reading the manuscript.

References

Birtill, J.W., and F.E. Whiteway, 1965. Phased seismometer arrays. *Phil. Trans. R. Soc.* A, 258, 421.

Mack, H., 1969. The deconvolution of LASA short-period seismograms. *Trans. AGU.* 50, 245 (abstract only).

Manchee, E.B., and H. Somers, 1966. The Yellowknife seismological array. *Pub. Dom. Obs.* 32, 2.

Manchee, E.B., and D.H. Weichert, 1968. Epicentral uncertainties and detection probabilities from the Yellowknife seismic array data. *Bull. Seism. Soc. Am.* 58, 1359.

Somers, H., and E.B. Manchee, 1966. Selectivity of the Yellowknife seismic array. *Geophys. J.,R. Astr. Soc.* 10, 401.

Weichert, D.H., 1969. The measurement of $dT/d\Delta$ with the Yellowknife seismic array. *Trans. AGU* 50, 244 (abstract only).

Weichert, D.H., E.B. Manchee, and K. Whitham, 1967. Digital experiments at twice real-time speed on the capabilities of the Yellowknife seismic array. *Geophys. J.,R. Astr. Soc.* 13, 277.

Weichert, D.H., and E.B. Manchee, 1969. A photogrammetric re-survey of the Yellowknife seismic array. *Seism. Series, Dom. Obs.* 1969-2.

Weichert, D.H., and K. Whitham, 1969. Calibration of the Yellowknife seismic array with first zone explosions. *Geophys. J.,R. Astro. Soc.*, 18, 461.

Wilson, A.J.C., 1965. The location of peaks. *Brit. J. Appl. Phys.* 16, 665.